# The capacitance of pristine ice crystals and aggregate snowflakes

CHRISTOPHER D. WESTBROOK, ROBIN J. HOGAN AND ANTHONY J. ILLINGWORTH

Department of Meteorology, University of Reading, UK.

March 14, 2019

### ABSTRACT

A new method of accurately calculating the capacitance of realistic ice particles is described: such values are key to accurate estimates of sublimation rates in numerical weather models. We have directly simulated the trajectories of diffusing water molecules, using random 'walkers'. By counting how many of these trajectories intersect the surface of the ice particle (which may be any shape) and how many escape outside a spherical boundary far from the particle, we have estimated the capacitance of a number of model ice particle habits including hexagonal columns and plates, 'scalene' columns and plates, bullets, bullet-rosettes, dendrites, and realistic aggregate snowflakes. For ice particles with sharp edges and corners this method is an efficient and straightforward way of solving Laplace's equation for the capacitance. Provided that a large enough number of random walkers are used to sample the particle geometry ( $\sim 10^4$ ) we expect the calculated capacitances to be accurate to within  $\sim 1\%$ . The capacitance for our modelled aggregate snowflakes  $(C/D_{max}=0.25,$  normalised by the maximum dimension  $D_{max}$ ) is shown to be in close agreement with recent aircraft measurements of snowflake sublimation rates. This result shows that the capacitance of a sphere  $(C/D_{max}=0.5)$  which is commonly used in numerical models, overestimates the evaporation rate of snowflakes by a factor of two.

We have also investigated the effect of vapor 'screening' by crystals growing in the vicinity of one another, and the results clearly show the difficulties in accurately estimating crystal growth rates from laboratory experiments. The reduction in vapor supply caused by this screening is found to significantly reduce the capacitance compared to a crystal growing in isolation, by a factor of three in our model setup.

## 1. Introduction

The growth and evaporation of ice particles by diffusion of water vapor on to and away from the surface of ice particles are fundamental processes for the development of ice clouds and precipitation. The density of water vapor  $\rho$  around such an ice particle is governed by Laplace's equation:

$$\nabla^2 \rho = 0, \tag{1}$$

under quasi-steady-state conditions (Pruppacher and Klett 1997). Typically the separation between ice particles in a cloud is such that each ice particle may be considered in isolation against a background vapor density  $\rho_{\infty}$ . If the vapor density at the surface  $\rho_s$  is assumed to be constant, this leads to the growth rate:

$$\frac{\mathrm{d}m}{\mathrm{d}t} = D \int_{s} \nabla \rho \cdot \mathrm{d}\mathbf{s} = 4\pi DC(\rho_{\infty} - \rho_{s}), \qquad (2)$$

by application of Gauss's law over the particle surface s, where D is the diffusion coefficient for water vapor, and the capacitance C characterizes the shape and size of the ice particle.

The assumption of constant  $\rho_s$  implies a constant surface temperature. The temperature  $T_s$  at any given part of the surface is determined by both the flux of vapor on to that part of the crystal, resulting in the release of latent heat; and by the rate at which that heat is conducted away from the crystal. Since the equations for diffusion of vapor and transport of heat take the same form, even if a portion of the surface has a larger flux of vapor on to it and becomes hotter through the release of latent heat, it should lose that extra heat at a correspondingly higher rate, resulting in a constant temperature across the whole particle surface.

The assumption of constant  $\rho_s$  motivates an analogy with electrostatics, where the results for the capacitance C are well known for simple geometries (see table 1). However, exact solutions for the non-smooth shapes of natural ice particles are not available, and in numerical models (eg. Wilson and Ballard 1999) a capacitance based on one of the shapes in table 1 is usually applied in its place. It is far from clear whether this approximation is a reasonable one, or what the capacitance of realistic ice particles actually is, particularly for large particles which may be complex aggregates. Chiruta and Wang (2003) suggested a refinement to this situation by approximating bullet rosette crystals by a set of smooth lobes and solving equation 1 numerically using a finite-element method to obtain the vapor density  $\rho$  around the particle, and capacitance C. Recently, the same authors have also applied this procedure to solid and hollow columns, estimating the capacitance for five model aspect ratios (Chiruta and Wang 2005). McDonald (1963) used metal models of ice particles to simulate

<sup>\*</sup>Corresponding author address: Dr. Chris Westbrook, Department of Meteorology, University of Reading, Berkshire, RG6 6BB, UK; email c.d.westbrook@reading.ac.uk

Table 1: Theoretical capacitances for simple shapes (McDonald 1963) . Note that electrical capacitances (in Farads) are usually normalised as  $4\pi\epsilon C$ , where  $\epsilon$  is the permittivity of the surrounding medium in Fm<sup>-1</sup>.

Shape	Capacitance
Sphere, radius $r$	C = r
Thin disc, radius $r$	$C = 2r/\pi$
Prolate spheroid: major,	$C = A/\ln[(a+A)/b],$
minor semiaxes $a, b$	where $A = \sqrt{a^2 - b^2}$
Oblate spheroid: major,	$C = ae/\sin^{-1}e,$
minor semiaxes $a, c$	where $e = \sqrt{1 - c^2/a^2}$

ice particles and made measurements of their capacitance, however the presence of the connecting wire combined with the small magnitude of the capacitances involved limits the accuracy of such an approach.

In this paper we describe a new method for calculating the capacitance of realistic ice particles. We use a Monte Carlo approach, directly sampling the trajectories of diffusing water molecules onto the surface of an ice particle. For the non-smooth shapes of realistic ice particles, this turns out to be an efficient method of solving Laplace's equation and accurately estimating C. Also, since we are sampling steadystate diffusion, we are able to build up the statistics for C by sampling one water molecule trajectory at a time, and this means that very little computer memory is required. It is interesting to note that random walker sampling has recently been applied in the electrostatics community to solve Laplace's equation and calculate electrical capacitances for conductors with sharp edges (eg. Hwang and Mascagni 2004) since it bypasses many of the artefacts introduced by boundary-element, finite-difference and finite-element methods which can cause systematic errors (Wintle 2004).

In this work we have sampled the capacitance of a number of model pristine ice crystal types, as well as aggregate snowflakes. These shapes are much more realistic than those that are used in numerical models at present, and therefore we should have much more confidence that the results given here accurately represent the capacitance of natural ice particles. This is very important if quantitative comparisons are to be made between observations and model predictions of deposition and evaporation (eg. Forbes and Hogan 2006).

## 2. Method

The simplest Monte Carlo model for solving (1) runs as follows. A random walker is placed on a

large sphere, radius  $R_{\infty}$ . Its position is chosen at random with uniform probability over the sphere's surface. This represents the far-field where the surfaces of equal vapor density are spherical. Once released from this sphere, the walker is allowed to diffuse around, taking steps much smaller than any characteristic length scales in the target ice particle. Each step is taken in a random direction. The walker's motion is tracked until either i) it hits the surface of the particle, or ii) it escapes outside the large sphere  $R_{\infty}$ (where the 'background' vapor density  $\rho_{\infty}$  is fixed). Note that we have treated the ice particle as a perfect absorber with  $\rho_s = 0$ , but from (2) we see that our calculated capacitances will be valid for any value of  $\rho_s$  (including both deposition and evaporation) provided that it is constant over the ice particle surface. The process is repeated for a large number of walkers until an accurate sample of hits and misses has been obtained: then the capacitance may be calculated as  $C = fR_{\infty}$  where f is the fraction of walkers that hit the target. We emphasize that the values of the capacitance C estimated using the above method are the same irrespective of the particle surface vapor density/temperature: the capacitance is a function of the shape and size of the particle alone, provided that  $\rho_s$  and  $T_s$  are constant.

In practice, the method outlined above is very inefficient, with a large amount of time being spent tracking the walkers as they take very small steps through large regions of empty space. To improve the method, we use the fact that the probability distribution for the trajectories of random walkers which encounter no obstacles is isotropic: this allows us to make a number of significant improvements to the algorithm. The first improvement is to start the walkers on a sphere much closer to the particle, with radius R such that this sphere just encloses the particle, as illustrated in figure 1. Because the random walkers released from  $R_{\infty}$  encounters no obstacles between  $R_{\infty}$  and R, starting the walkers with a uniform distribution over the surface of this much closer sphere introduces no bias at all on the statistics. The only condition is that if the walkers move outside R we must track them all the way to the outer boundary  $R_{\infty}$  before assuming that they have gone to infinity. However, this is not a great burden: if a walker finds itself outside of R, we can let it take large steps (as large as the shortest distance back to the sphere R), since we can be sure it will encounter no obstacles over this step length. We emphasise that this does not force the vapor density profile at radius Rto be spherical (which we would be incorrect); we are simply using the fact that the density of walkers which start from  $R_{\infty}$  and diffuse around until they reach R does have a spherical profile (because they

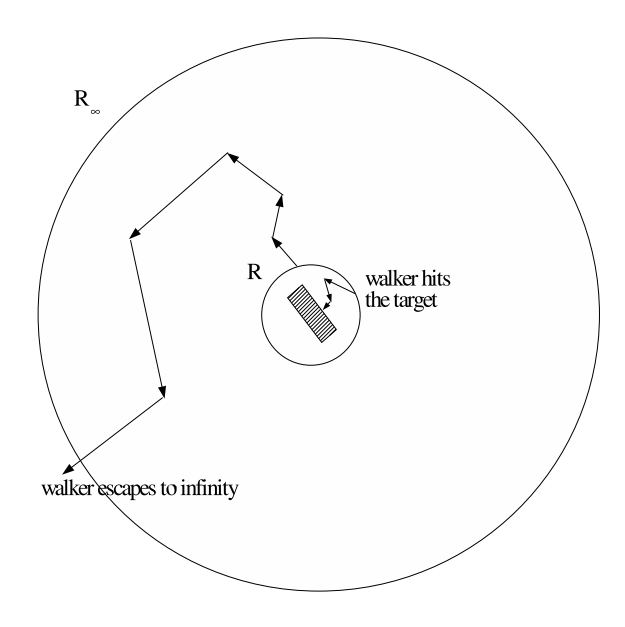


Fig. 1: Diagram illustrating the random walker method. Walkers start from the sphere R enclosing the particle, and are tracked along a random walk until they i) hit the particle, or ii) escape beyond a distant spherical outer boundary  $R_{\infty}$ . Note that outside R the walker is able to take big jumps without any change in its statistics; inside R, the walkers can take a jump equal to the distance to the closest point on the surface of the ice particle. In both cases the jumps are in random directions.

have not yet had a chance to hit the ice particle, so their statistics cannot have been affected by it). This improvement allows us to reduce the time spent following the movement of the walker whilst it is far from the particle, without altering the statistics of how many walkers hit the particle at all.

While the walker is inside the sphere R we must be more careful. We can still optimize the step length of our walkers though, by calculating the minimum distance from the walker to the closest point on the ice particle after each step, and setting this distance to be the length of the next step. We assume that the walker has hit this ice particle if it comes within some small distance  $\epsilon$  of one of the surfaces. Again, we repeat the whole process for a large number of walkers so that we may accurately sample the particle's capacitance, which is now given by C = fR.

The accuracy of the method described above is determined by three factors: i) the number of walkers used; ii) how far away the 'infinite' boundary  $R_{\infty}$  is placed; and iii) the thickness of the thin absorbing layer  $\epsilon$ . In our calculations we have set the outer boundary condition to be  $R_{\infty} = 500R$ , and the absorption layer thickness  $\epsilon$  is set to be less than 0.1% of the smallest side length of any of the faces on the particle. There are alternative methods that bypass the construction of such a layer (Mascagni and

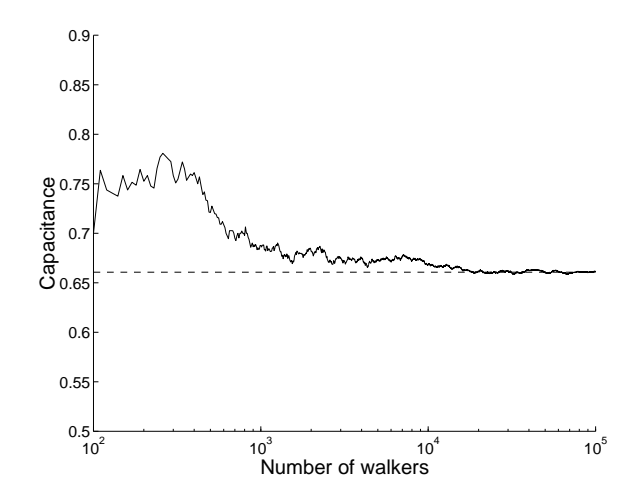


Fig. 2: Capacitance of unit cube as sampled by an increasing number of random walkers. Dashed line shows the theoretical value of 0.6607 (to 4 d.p.) as calculated by Hwang and Mascagni (2004). The outer boundary was set at  $R_{\infty}=500R$ , and the thickness of the absorption layer was  $\epsilon=0.001$  (0.1% of the side length).

Hwang 2003); however, for our purposes, simply using a small value of  $\epsilon$  should be sufficient. To test the accuracy of the method, we have used it to calculate the capacitance of a unit cube, which is known to within a tolerance of  $10^{-7}$  (Hwang and Mascagni 2004). Provided a large number of walkers are used (>  $10^4$ ), the calculation using our method shows excellent agreement to well within 1% of this established value, as shown in figure 2. Sensitivity show indicate that increasing  $R_{\infty}$  to a value of 1000R has no effect on the estimated capacitance to within  $\sim 0.1\%$ .

We have also tested our algorithm against particles where the analytic solution is known (see table 1). For a thin circular disc with unit radius and thickness of 0.001, we estimate the capacitance to be C=0.639, which matches the exact analytical result for an infinitely thin disc ( $C=2/\pi=0.637$ ) to within 1%. For a unit sphere we find that our method also agrees with the theoretical value (C=1) to well within 1%. In both cases  $10^4$  walkers were used.

## 3. Results

Having established that the method is accurate, we proceed to apply it to a number of model ice particle habits, and the results of this are described below.

# a. Hexagonal columns and plates

Close to cloud top, one of the most common pristine ice crystal habits is the hexagonal prism (Pruppacher and Klett 1997). We have used our random walker method to calculate the capacitance of these particle shapes, and two examples of this kind of crys-

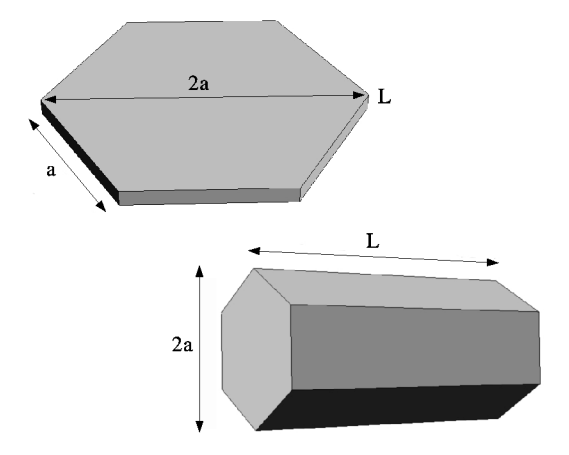


Fig. 3: Geometry of pristine hexagonal column and plate ice particles. Width 2a defined as maximum span across basal (hexagonal) face; length L is the thickness of the plate, or length of the column (ie. the maximum span of the particle in the direction perpendicular to the basal face).

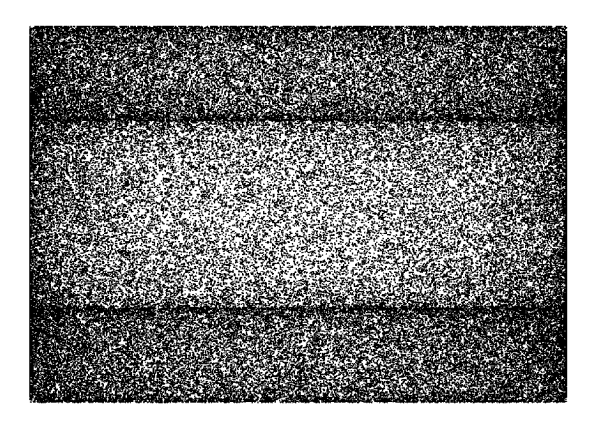


FIG. 4: Impact positions of random walkers from our simulations onto the surface of a hexagonal column, as viewed in projection from the side. The flux of walkers is highest on the sharp edges and corners of the particle, where the vapor density gradient is largest.

tal (a column and a plate) are shown in figure 3. We define the width 2a to be the maximum span across the basal (hexagonal) crystal face, and the length L as the span of the crystal perpendicular to the basal face. We also define the aspect ratio of the crystal as  $\mathcal{A}=L/2a$ : hexagonal columns correspond to  $\mathcal{A}>1$ , plates to  $\mathcal{A}<1$ .

We used 250,000 walkers to sample the capacitance of the crystals, and estimate that our results for C are accurate to within 1%. The distribution of random walkers incident on the faces of a column are shown in side projection in figure 4: as one would expect from equation 1, walkers impact on the particle all across the surface, but are most concentrated around the sharp edges and corners where we expect the vapor density gradient  $|\nabla \rho|$  to be highest.

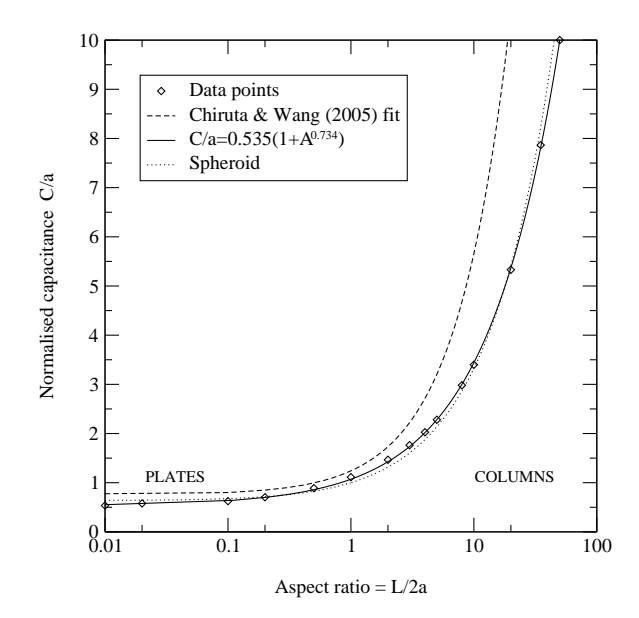


FIG. 5: Capacitance of hexagonal columns and plates with aspect ratios between  $\mathcal{A}=0.01$  (thin plates) and  $\mathcal{A}=50$  (thin columns). Diamonds are data points from our calculations in units of a. Solid line is fitted curve  $C/a=0.535(1+\mathcal{A}^{0.734})$ . Dashed line shows the fit suggested by Chiruta and Wang (2005). Dotted curve is the capacitance of a spheroid with major and minor axes chosen to match the length L and basal span 2a of the crystal.

Figure 5 shows the capacitance of hexagonal prisms calculated for a constant width (a = 1), where we have varied the aspect ratio between 0.01 and 50. We have fitted a curve to our data points and have found that the equation:

$$C = [0.535 (1 + \mathcal{A}^{0.734})] a \tag{3}$$

closely approximates our data to within  $\sim 3\%$ ; this curve is overlaid in figure 5 for comparison. Also shown in figure 5 is the fitted curve derived for hexagonal columns and plates by Chiruta and Wang (2005) using a finite-element method. They proposed a linear fit C = (0.751 + 0.491A)a, and this is plotted in figure 5 for comparison with our results. Over the range of aspect ratios they considered (A = 0.2 to 3.33) their results are 20–30% higher than our calculated values. The source of this discrepancy between their data points and ours most likely lies in the positioning of the outer boundary: in Chiruta and Wang's finite-element calculations it was placed at a distance of  $\sim 10$  particle radii; our random walker method has allowed us to place it much further away, at a distance of 500 radii. Sensitivity analysis (M. Chiruta – personal communication) indicates that if the outer boundary in their finite-element method is placed too close to the particle, the estimated capacitances are systematically higher than their true values. The position of the outer boundary is a parameter to which capacitance results are surprisingly sensitive: this issue was also encountered in the experiments of Mc-Donald (1963) who found that the measured capacitance of metal ice particle models (smaller than 5cm) placed inside a 1m Faraday cage were sensitive to the position of the model inside the cage.

The final curve plotted on figure 5 shows the results for spheroids with major and minor axes matched to the length and maximal basal span of the crystal, and gives reasonable agreement over the whole range of aspect ratios considered here (relative error: +20% for A = 0.01; -3% for A = 1; +9% for A = 50). This is at odds with Chiruta and Wang's conclusion that spheroids always provided a significant underestimate of the capacitance of hexagonal columns, but from the above discussion it seems clear that this is because their method overestimated the capacitance of those hexagonal columns. We note that although their absolute values of C are overestimates, Chiruta and Wang's main conclusion that solid and hollow columns have almost identical capacitances to one another should still be correct.

We have compared the capacitance of thin hexagonal plates to that of a thin circular disc. The measurements of McDonald (1963) indicated that a disc with the same surface area is a reasonable approximation for the capacitance of a plate. This is backed up by our calculations, where we find that a plate with  $\mathcal{A}=0.01$  has a capacitance of C/a=0.535, compared to the equivalent-area disc which has  $C/a=0.91\times 2/\pi=0.579$  (8% higher).

## b. 'Scalene' columns and plates

It has been observed (Bailey and Hallett 2004) that the basal faces of columns and plates are not always perfect regular hexagons, but are often somewhat distorted. Here we calculate the capacitance of two so-called 'scalene' forms similar to those reported in that paper, and assess the impact of breaking the perfect hexagonal symmetry. The shapes of the model scalene basal faces considered here are shown in figure 6. In both cases the maximum span across the basal face is defined as 2a, and the aspect ratio  $\mathcal{A}$  is defined as before. We calculate the capacitances of these scalene crystals for three aspect ratios:  $\mathcal{A} = 0.1$ ,  $\mathcal{A} = 1$  and  $\mathcal{A} = 10$ , and compare the results with a perfect hexagonal crystal of the same maximum basal span and length.

The basal face of the first scalene crystal is a 'flattened' hexagon, with 4 short sides and 2 longer sides, and a width perpendicular to the maximum basal span of a (compared to  $\sqrt{3}a$  for a regular hexagon). The internal angles are all 120°. For  $\mathcal{A}=0.1$  and  $\mathcal{A}=1$  we find that C is reduced by approximately 10% relative to a regular hexagonal column. For

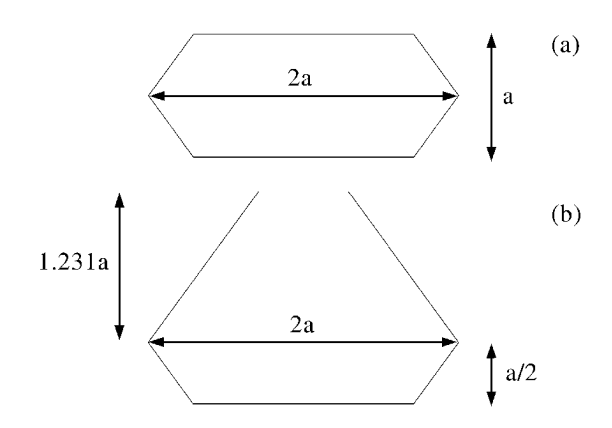


FIG. 6: Geometry of basal faces for the distorted or 'scalene' hexagonal columns and plates. For both types the maximum span across the basal face is defined as 2a and all of the internal angles are  $120^{\circ}$ . The model shapes are: (a) a 'flattened' hexagon with 4 short sides and 2 longer sides; (b) a second scalene type with 3 short sides and 3 longer sides.

 $\mathcal{A}=10$  the capacitance is only 2% lower than the regular column.

The second model scalene crystal type has 3 short sides and 3 long sides, with a span between opposite sides of  $\sqrt{3}a$  (the same as for a regular hexagon). For this type we found that C is essentially identical to a regular column/plate for all three aspect ratios, to within 4%. We conclude that distortion of the hexagonal geometry of the crystals has a relatively small impact on their capacitance, and the only significant difference in the growth/evaporation rates is likely to be from surface/crystalline effects which are not included here.

#### c. Bullets and bullet-rosettes

Bullets and bullet-rosettes are one of the most common crystal habits in cirrus clouds (Heymsfield and Iaquinta 2000). Here we consider some simple model bullets and bullet-rosettes as illustrated in figure 7. The bullets are modelled by a hexagonal column of length L, width 2a, with an hexagon-based pyramid attached to one of one end. We define P as the ratio of the height of the pyramid cap relative to the column length, and in what follows we will assume a value of  $\frac{1}{2}$ . We define the aspect ratio  $\mathcal{A} = L/2a$ , as before.

We have calculated the capacitance of single bullets with different thicknesses corresponding to aspect ratios  $\mathcal{A}$  between 1 and 10. The measured capacitances are plotted in figure 8. Equation 3 for hexagonal columns of the same width (=2a) and total length (=L+PL) is also plotted on the figure. Comparison between the two shows that our model bullets have a capacitance which is reduced by a uni-

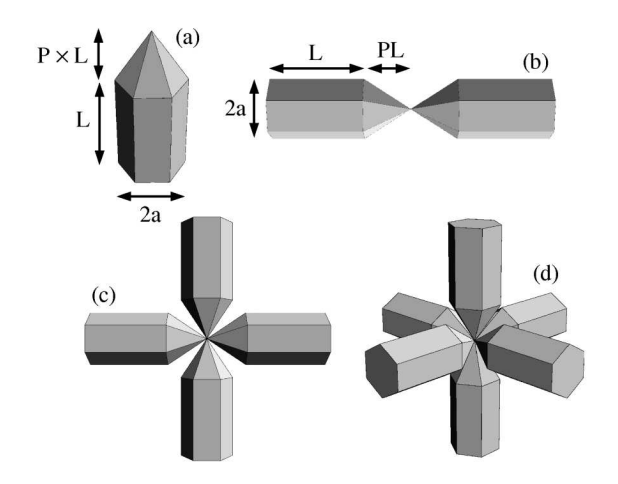


Fig. 7: Model geometry for: a) single bullet, b) 2-rosette, c) 4-rosette and d) 6-rosette crystal types.

form 7.5% compared to that of a column. Reducing the size of the pyramid cap to  $P=\frac{1}{4}$  (following Macke et~al~1996) we find the capacitance is now only 5.5% lower than that the complete column, and further reductions in P result in an asymptotic approach to the capacitance of a simple column.

Three model rosettes were constructed, and these are illustrated in figure 7. The '2-rosette' is simply a linear combination of the two bullets, joined at the tip. Calculations for a range of aspect ratios in the range  $\mathcal{A}=1$  to 10 indicate that the capacitance of the 2-rosette is essentially identical a solid column of the same overall length and breadth, and given the geometry, this is not surprising.

The '4-rosette' has 4 bullets lying in a plane, each neighbouring bullet seperated by 90°. Due to the more complex geometry of this crystal shape, we have calculated its capacitance relative to the maximum dimension  $D_{max}$  (rather than the bullet width) for a variety of aspect ratios: these values are shown in figure 9. We have fitted the curve:

$$C = 0.35 \mathcal{A}^{-0.27} D_{max},\tag{4}$$

which appears to provide a close approximation to the data. Also shown in figure 9 is the capacitance of an oblate spheroid with major and minor axes matched to the overall dimensions of the rosette (major axis =2L+2LP, minor axis =2a) and this curve overestimates the capacitance quite severely except when the aspect ratio of the bullets is close to unity. We also show the values for a disc (see table 1) with the same maximum dimension, and this also overestimates the capacitance for aspect ratios larger than  $\simeq 1.5$ . A sphere with the same maximum dimension is found to overestimate the capacitance by more than a factor of two for rosettes of thin bullets.

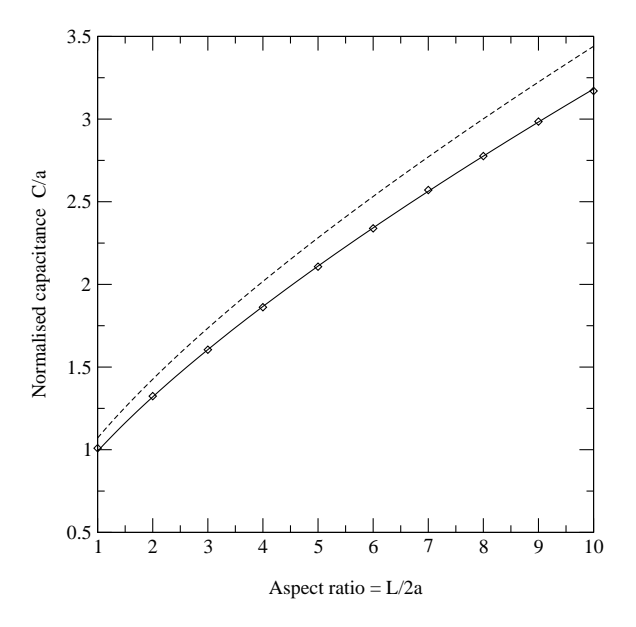


FIG. 8: Capacitance of single bullet crystals as a function of aspect ratio. Diamonds are data points from our calculations in units of a. Dashed line shows equation 3 for hexagonal columns of the same width and total length as the bullet; solid

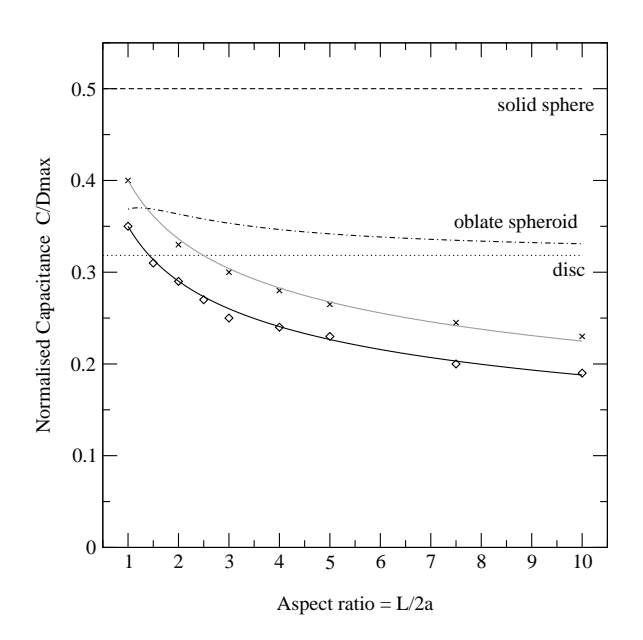


FIG. 9: Capacitance of bullet-rosette crystals as a function of the aspect ratio of the arms  $\mathcal{A}=L/2a$ . The capacitances are normalised relative to the maximum dimension of the rosette  $D_{max}$ . Diamonds are the modeled values of C for the 4-arm rosette; crosses are the values for the 6-arm rosette. Solid black and gray lines are the respective fitted curves (see text). The dashed line shows value of C for a sphere of the same maximum dimension; the dotted line shows value for a thin disc. The capacitance of an oblate spheroid with a major axis of P(1+L) and minor axis of 2a is shown by the dash-dot line.

The final model crystal is a '6-rosette' made of six bullets in a three-dimensional cross shape, each seperated from its neighbours by an angle of  $90^{\circ}$ . The data for this rosette is also shown in figure 9 and the capacitances are approximately 15% higher than for the 4-bullet rosette. We have fitted a curve to this data, and find that

$$C = 0.40 \mathcal{A}^{-0.25} D_{max} \tag{5}$$

is a good approximation to it. Again, a sphere of the same maximum dimension strongly overestimates the capacitance at all aspect ratios; a disc provides a closer approximation, but still overestimates the capacitance at large aspect ratios.

#### d. Dendrites

We have constructed two model dendrite crystal types. The first is a simple six-armed star shape, where each arm is a 'flattened' hexagonal plate similar to those described in section (3b). Each of these arms is separated from its neighbours by an angle of  $60^{\circ}$ . The arms overlap at the centre of the crystal, and the internal angles of the arms are all  $120^{\circ}$ . The span between the tips of two opposite arms is defined as 2a, and the thickness is fixed as (2a)/100. The width of the arms is characterised by the ratio  $\mathcal{A}' = w/a$  which we define as the ratio of the separation between the two longest sides of the hexagon w to the arm length a. These dimensions are marked on figure 10, which shows the distribution of impacting walkers for a star crystal with  $\mathcal{A}' = 0.2$ .

The capacitance of our stars as a function of the width of the arms is shown in figure 11. For a star with thin arms ( $\mathcal{A}'=0.01$ ) the capacitance is 40% lower than a hexagonal plate of the same overall dimensions (C=0.535a). As the arms become thicker, the capacitance rises and asymptotically approaches the value for a solid plate. The curve:

$$C = 0.535(1 - 0.40e^{-7.53A'})a,$$
(6)

is also plotted in figure 11 and approximates the data to within a few percent.

The second model is an adaptation of the star model above, where we have added a pair of secondary branches to each arm, each with one third the dimensions of the main arms. These secondary branches are positioned with one end at the centre of the main arm, and oriented at an angle of  $60^{\circ}$  on either side of it. Figure 10 also shows the distribution of impacting walkers on this crystal type, with A' = 0.05.

We have calculated the capacitance of this model crystal for different arm thicknesses, and the data is shown alongside the results for the star shapes in

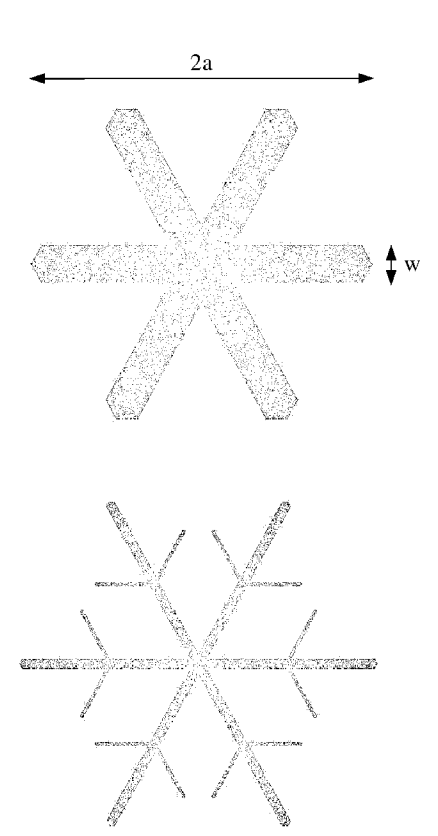


Fig. 10: Distribution of walkers impacting on the surface of star-type crystal (top) and dendrite with secondary branches (bottom).

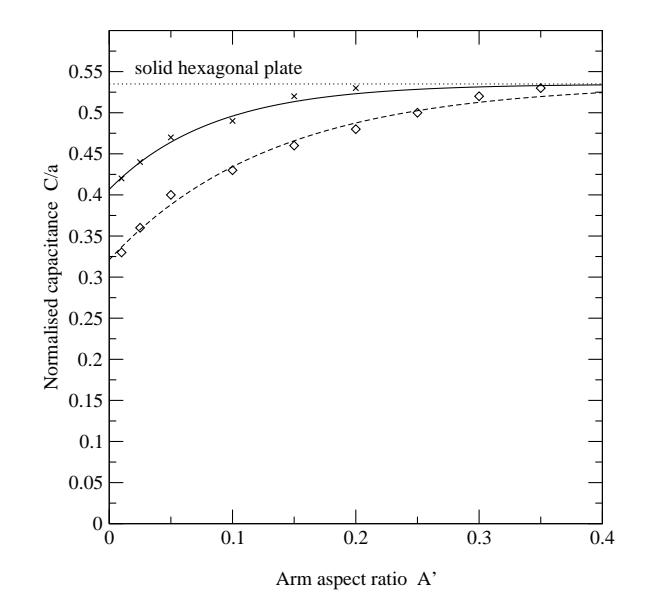


FIG. 11: Capacitance of dendrite crystal types. Diamonds are for simple star shapes, crosses are for branched types. The capacitance of a solid hexagonal plate of the same overall dimensions is indicated by the dotted line. Dashed and solid lines are fitted curves for star and branched crystal data respectively (see text).

figure 11. Adding the branches increases the capacitance quite significantly for dendrites with thin arms (for  $\mathcal{A}'=0.01$  the branched dendrite has a capacitance  $\sim 30\%$  larger than a star). As the branches become thicker they again approach the value for a solid plate. We have fitted a curve to the data:

$$C = 0.535(1 - 0.24e^{-11.9A'})a, \tag{7}$$

and this function approaches the solid plate limit rather faster than the simple star crystal.

### e. Aggregates

In this section we consider aggregates of the above ice crystal types. Aggregates are often the dominant particle habit in deep non-precipitating cirrus clouds (Field and Heymsfield 2003, Westbrook et al 2006), as well as in snowstorms (Jiusto and Weickmann 1973). A recent theoretical model of ice crystal aggregation (Westbrook et al 2004) has allowed us to produce large samples of realistic 'synthetic' ice aggregates. In this section we have calculated the capacitance of these synthetic snowflakes in the expectation that the results ought to be a good approximation to the capacitance of natural ice aggregates.

We applied our method to  $\sim 1000$  synthetic aggregates sampled from the simulations of Westbrook et al (2004): a few examples are shown in figure 12. We have calculated the average capacitance of the synthetic aggregates, using  $10^3$  walkers to sample each individual aggregate. We note that this is a smaller number of walkers than was used for the pristine ice crystal habits; however, we are averaging the results over several different realisations of the aggregate geometry (every aggregate snowflake is different), so we expect that our eventual statistics should be accurate. In any case the results for the unit cube in section 2 indicate that the error in the calculated values for each individual aggregate should be less than 10%.

For each aggregate, the ratio of capacitance to maximum dimension  $C/D_{max}$  was calculated, and the results binned and averaged as a function of the number of crystals in the aggregate: this is shown in figure 13. The 'monomer' crystals in this case were hexagonal columns with an aspect ratio of A = 2. The capacitance of the monomer columns is  $C/D_{max} =$ 0.319 (see section 3a), but for an aggregate of just two columns this is reduced to  $0.21 \pm 0.02$ , since two columns stuck together is a much more open geometry than a single column. As more columns are aggregated the normalised capacitance rises to an asymptotic limit of  $0.25 \pm 0.02$ . This value is in strong agreement with recent in-situ aircraft measurements of aggregate snowflake sublimation made by Field et al (2006) during a Lagrangian descent through a subsaturated portion of an ice cloud, where a value of



Fig. 12: Examples of aggregates made up of 2,4,10 and 32 hexagonal columns, sampled from the simulations of Westbrook *et al* (2004). The aspect ratio of the columns is A = 4.

 $C/D_{max} = 0.23$  was found.

We have repeated the calculations for different monomer aspect ratios, and this is shown in figure 14. We find that irrespective of the monomer shape the normalised capacitance approaches an asymptotic value of between 0.25 (thin columns  $\mathcal{A}=8$ ) and 0.28 (squat columns  $\mathcal{A}=1$ ). Changing the monomer crystal type to bullet-rosettes rather than columns is found to have very little effect on the capacitance, again yielding asymptotic values in the same range. This capacitance is smaller than a disc or sphere of the same maximum dimension, and the implication is that numerical models which assume these simple shapes are overestimating the growth/evaporation rate, by a factor of two in the case of the sphere.

It may perhaps appear counter-intuitive that the capacitance of aggregates should approach a constant value relative to their maximum dimension  $(C/D_{max} = constant)$ . The structure of the aggregates approaches a fractal geometry (Westbrook et al 2004) and as a result becomes increasingly open as the aggregates grow to contain more and more ice crystals. Because of this, the effective density decreases with size as  $(D_{max})^{-1}$  (in agreement with experimental data: Brown and Francis 1995, Heymsfield et al 2002). One might therefore anticipate that  $C/D_{max}$  would be reduced for large aggregates, since there is more empty space within a radius  $D_{max}/2$  of the particle centre, and therefore (one would imagine) more opportunity for a water molecule coming within that radius to escape. However, the results of Ball and Witten (1984) show that water molecules

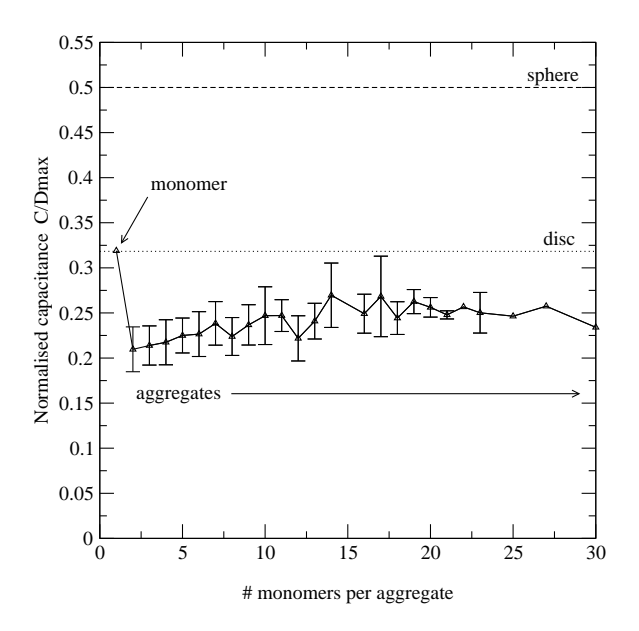


FIG. 13: Capacitance of aggregate snowflakes as sampled from the simulations of Westbrook et al (2004). The monomer crystals were hexagonal columns with  $\mathcal{A}=2$ . The calculated values of  $C/D_{max}$  were binned and averaged as a function of the number of crystals per aggregate, as shown on the horizontal axis. Error bars are one standard deviation, points with no error bar indicate the value for a single aggregate. The normalised capacitance asymptotically approaches a value of  $C/D_{max} \simeq 0.25$ . Overlaid are theoretical values for a sphere (dashed line) and a thin disc (dotted line) with the same maximum dimension.

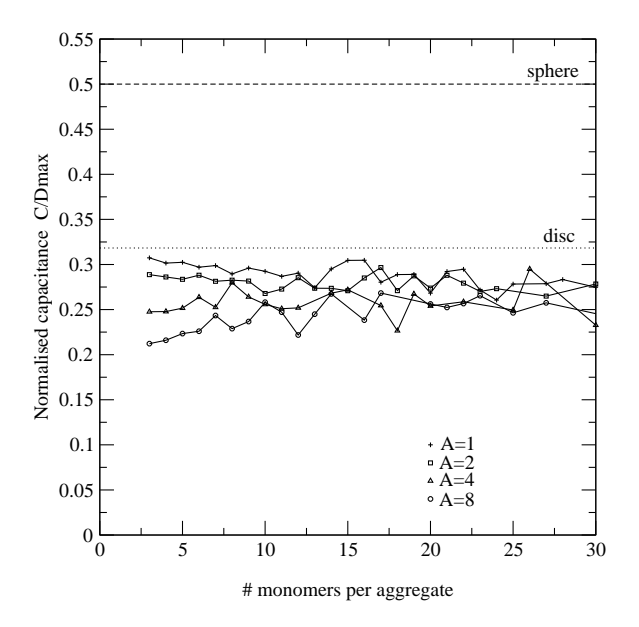


Fig. 14: The capacitance of aggregates with different monomer ratios  $\mathcal{A}$  between 1 and 8. All of the curves approach an asymptotic value in the range 0.25–0.28.

following a Brownian path are exceptionally efficient at exploring three dimensional space, and because of this the ice particle appears essentially opaque to the incident water molecules (i.e. a fixed fraction of those venturing within  $D_{max}/2$  will be absorbed). As a result,  $C/D_{max} = \text{constant}$  is in fact the physically sensible result for aggregates (see appendix for further details).

## 4. Screening

Growth rates derived from laboratory experiments such as those of Bailey and Hallett (2004) are usually measured from crystals which grow not in isolation, but surrounded by other growing crystals. Screening of one ice crystal by another may be an important effect in light of the above discussion on aggregates, since the diffusing water molecules are very efficient at exploring the space around the particle, so neighbouring crystals may constrict the vapor supply to one another. An understanding of such screening effects is important if laboratory data are to be accurately interpreted.

For our model setup we consider 8 identical hexagonal columns with A = 5 in a 'spiral staircase' geometry, growing with their longest axis in the horizontal direction. Neighboring crystals are offset in the vertical direction by a column's width and are rotated around the vertical axis by 45°. This is shown in figure 15 and is roughly modelled after photographs of experimental setup in Bailey and Hallett (2004). We used  $10^4$  walkers to sample the capacitance of these crystals, and found that the vapor supply to the innermost crystals is inhibited to such an extent that their capacitance is reduced to approximately one third of its value for a single column in isolation  $(C/a \simeq 0.75 \text{ compared to } 2.28 \text{ in isolation}).$ This result demonstrates how sensitive the vapor field around a crystal is to other sources/sinks of vapor in the vicinity. It also shows that if the growth rates from experiments are to be compared to theoretical capacitances, the crysals must be grown in isolation, or separated from one another as much as possible. Electrodynamic trapping techniques (eg. Swanson et al 1999) where ice particles are levitated in an electric field and allowed to grow in isolation may be useful in this respect, although to the authors' knowledge the results have so far been limited to small particles, less than  $100\mu m$  in size.

### 5. Discussion

The capacitance for pristine ice crystals and aggregate snowflakes has been calculated using a new Monte Carlo method, and these new values should be an improvement on the traditional approximations of

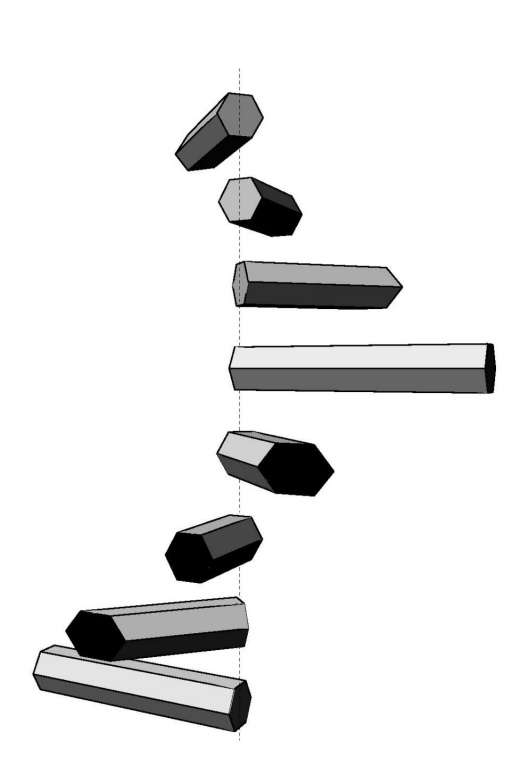


Fig. 15: Model 'laboratory' setup of 8 identical hexagonal column crystals. Each is rotated by an angle of  $45^{\circ}$  about the vertical axis relative to its neighbours, and offset in the vertical direction by a crystal's width, in an attempt to model crystals growing on a vertical filament (indicated by the dotted line). The growth rate of the innermost crystals is approximately one third the growth rate of a column growing in isolation.

smooth spheroids or discs. Application of these capacitances to estimate the actual growth/evaporation rates requires a prescription for the difference between the surface and the far-field vapor densities  $(\rho_s - \rho_\infty)$ . Using the Clausius-Clapeyron equation, an expression for dm/dt in terms of the supersaturation with respect to ice (S-1) is obtained:

$$\frac{\mathrm{d}m}{\mathrm{d}t} = 4\pi C \times \frac{S-1}{A+B} \tag{8}$$

where the parameters A(T) and B(T,P) are given in Pruppacher and Klett (1997) and depend on the ambient temperature T and pressure P. We believe that the results described in this paper may help to improve the estimation of growth and evaporation rates calculated in numerical weather prediction and cloud resolving models, especially for spatially extended particles such as bullet rosettes, dendrites and aggregates, where modelling the particle as a simple sphere (eg. the Met Office forecast model: Wilson and Ballard 1999) can overestimate |dm/dt| by a factor of 2. This work may also be valuable to new precipitation models which predict ice particle habit from the model temperature and humidity (eg. Woods et al 2006), allowing an appropriate capacitance to be used for each predicted habit.

The key limitation of the present study is the question of whether the growth and evaporation rates of ice crystals are simply dominated by the rate at which vapor impinges on/diffuses away from the ice crystal surface, or whether surface kinetics plays a significant role in limiting the growth/evaporation rates. For evaporation of ice particles, Nelson (1997) showed that the sublimation rate is controlled by (8) and that surface kinetics can be neglected. This conclusion is backed up by in-situ imaging of sublimating ice particles (Korolev and Isaac 2004) which indicate that the vapor flux away from the particles is concentrated at the corners and edges, as one would expect if equation (1) controls the vapor density. We therefore expect our results to be directly applicable to calculating the evaporation rates of natural ice particles.

For deposition, the growth of smooth surfaces under equation 1 alone is well known to be unstable (Langer 1980, Mullins and Sekerka 1963) and if the water molecules are simply 'stuck' rigidly at the point where they first impinge on the ice surface, fernlike fractal patterns result (Witten and Sander 1981, Bowler and Ball 2005). In reality the incident water molecules will undergo some rearrangement on the surface of the particle before being incorporated into the ice lattice; it also seems likely that some fraction of the water molecules incident on the surface will be rejected completely, depending on the crystal size and ambient conditions. For very small cold

crystals Magee  $et\ al\ (2006)$  reports that surface kinetic effects play a key role in controlling the growth, whilst for warmer dendrite crystal types the fern-like structure implies growth which is largely governed by the bulk diffusion of vapor, albeit with some anisotropy (Goold  $et\ al\ 2005$ ). For frozen drops, Korolev  $et\ al\ (2004)$  report that (8) is in good agreement with measured growth rates, and that the ice surface quickly develops roughnesses and protrusions, which one would expect given equation 1.

Recently, Bailey and Hallett (2004) compared the growth rates of laboratory-grown plate and column crystals (over a temperature range of -20 to  $-70^{\circ}$ C) to the growth rate calculated using (8), modelling their lab crystals as spheroids. Their results indicated that the predicted growth rates were only consistent with the measured values for aspect ratios close to  $A \simeq 1$ : for more extreme aspect ratios the theoretical values were as much as a factor of four too large for thin columns, and a factor of eight too large for thin plates. By contrast, they found that the growth rates were roughly proportional to the supersaturation, in agreement with (8). This sensitivity to the bulk excess vapor implies that the growth is not dominated by the surface kinetics; more likely is that a fraction of the impinging vapor cannot be incorporated into the lattice and is rejected from the surface.

Bailey and Hallett argue that because of the above discrepancy between predicted and measured growth rates, the whole approach of (8) is unsuitable for calculating deposition rates: their recommendation is that laboratory-measured growth rates should be used instead. However, the sensitivity of (1) to screening as discussed in section 4 show that their measured growth rates may be strongly affected by neighbouring crystals, restricting the vapor supply, and reducing the measured capacitance significantly (a factor of 3 in our model setup). The supporting glass filament may also play a significant role, particularly for thin columns where the filament thickness  $(50-70\mu m)$  is the same size or larger than the basal faces of the crystals. The interpretation of laboratory measured growth rates therefore requires a great deal of care, and this is an issue where further experiments and theoretical work are urgently required. Monte Carlo methods similar to the one presented here should be readily adaptable to incorporate surface kinetic effects when detailed data becomes available.

The capacitance of realistic ice aggregates has been calculated for the first time (to the authors' knowledge), and the results are in very close agreement with those estimated by Field *et al* (2006) from in-situ aircraft observations of sublimating ice aggregates, again indicating that (8) is a good approxima-

tion for sublimating ice particles. The authors believe that the capacitances presented here are, in any case, the best estimates currently available for the growth and evaporation of realistic ice crystals and snowflakes within the framework of the electrostatic analogy.

## **Appendix**

Here we show that  $C/D_{max}$  is a function only of the shape of an ice aggregate, and not its size. Imagine that the particle is removed and we replace it with a 'ghost' particle which is completely transparent to the diffusing water molecules. The average water molecule follows a Brownian trajectory, tracing a fractal path with dimension  $d_w = 2$  (Falconer 2003). This means that whilst the water molecule is within a distance  $D_{max}/2$  of the ghost particle centre, the resulting path fills a volume  $\propto (D_{max})^{d_w}$ . The ghost particle on the other hand, occupies a volume  $\propto (D_{max})^{d_i}$ , with  $d_i \simeq 2$  for our aggregates.

Since  $d_w + d_i > 3$ , the points where the particle and the uninterrupted random walk intersect with one another occupy a volume  $\propto (D_{max})^3$ . Because of this, the aggregates appear essentially opaque to the diffusing water molecules, in the sense that for a given monomer type, a fixed fraction of the molecules which venture within a radius  $D_{max}/2$  will come into contact with the ice particle. The ratio  $C/D_{max}$  simply represents this fraction, and is therefore independent of size.

### Acknowledgements

This work was funded by the Natural and Environmental Research Council (grant NER/Z/2003/00643). CDW acknowledges useful discussions with Paul Field (NCAR) and Mihai Chiruta.

### REFERENCES

Bailey, M. and J. Hallett 2004: Growth rates and habits of ice crystals between  $-20^{\circ}$ C and  $-70^{\circ}$ C. J. Atmos. Sci., **61**, 514–544

Ball, R. C. and T. A. Witten 1984: Causality bound on the density of aggregates. *Phys. Rev. A*, **29**, 2966–2967

Bowler, N. E. and R. C. Ball 2005: Off-lattice noise reduced diffusion-limited aggregation in three dimensions. *Phys. Rev. E*, **71**, 011403

Brown, P. R. A. and P. N. Francis 1995: Improved measurements of the ice water content of cirrus using an evaporative technique. *J. Atmos. & Ocean. Tech.*, **10**, 579–590

Chiruta, M. and P. K. Wang 2003: The capacitance of rosette ice crystals. J. Atmos. Sci., 60, 836–846

- Chiruta, M. and P. K. Wang 2005: The capacitance of solid and hollow hexagonal ice columns. *Geophys. Res. Lett.*, **32**, L05803
- Falconer, K. 2003, Fractal Geometry: Mathematical Foundations and Applications, 2nd Edition, John Wiley & sons, London.
- Field, P. R. and A. J. Heymsfield 2003: Aggregation and scaling of ice crystal size distributions. J. Atmos. Sci., 60, 544–560
- Field, P. R., A. J. Heymsfield and C. H. Twohy 2006: Capacitance of snowflakes. Submitted to J. Atmos. Sci.
- Forbes, R. M. and R. J. Hogan 2006: Observations of the depth of ice particle evaporation beneath frontal cloud to improve NWP modelling. Q. J. R. Meteorol. Soc., 132, 865–883
- Goold, N. R., E. Somfai and R. C. Ball 2005: Anisotropic diffusion-limited aggregation in three dimensions: universality and nonuniversality. *Phys. Rev. E*, **72**, 031403
- Heymsfield, A. J. and J. Iaquinta 2000: Cirrus crystal terminal velocities. J. Atmos. Sci., 57, 916–938
- Heymsfield, A. J., S. Lewis, A. Bansemer, J. Iaquinta, L. M. Miloshevich, M. Kajikawa, C. Twohy and M. R. Poellot 2002: A general approach for deriving the properties of cirrus and stratiform ice particles. *J. Atmos.* Sci., 60, 1795–1808.
- Hwang, C.-O. and M. Mascagni 2004: Electrical capacitance of the unit cube. *J. Appl. Phys.*, **95**, 3798–3802
- Jiusto, J. E. and H. K. Weickmann 1973: Types of snow-fall. Bull. Amer. Met. Soc., 54, 1148–1162
- Korolev, A. and G. A. Isaac 2004: Observations of sublimating ice particles in clouds. Proceedings of the 14<sup>th</sup> International Conference on Clouds and Precipitation, 808–811
- Korolev, A., M. P. Bailey, J. Hallett and G. A. Isaac 2004: Laboratory and in-situ observations of deposition growth of frozen drops. J. Appl. Met., 43 612–622
- Langer, J. S. 1980: Instabilities and pattern formation in crystal growth. Rev. Mod. Phys., 52, 1–28
- Macke, A., J. Mueller and E. Raschke 1996: Single scattering properties of atmospheric ice crystals. J. Atmos. Sci., 53, 2813–2825
- Magee, N., A. M. Moyle and D. Lamb 2006: Experimental determination of the deposition coefficient of small cirrus-like ice crystals near  $-50^{\circ}$ C. *Geophys. Res. Lett.*, **33**, L17813
- Mascagni, M. and C.-O. Hwang 2003:  $\epsilon$ -shell error analysis for 'walk on spheres' algorithm. *Math. & Comp. in Simul.*. **63.** 93–104

- McDonald, J. E. 1963: Use of the electrostatic analogy in studies of ice crystal growth. Z. Angew. Math. Phys., 14, 610–620
- Mullins, W. W. and R. F. Sekerka 1963: Morphological stability of a particle growing by diffusion or heat flow. J. Appl. Phys., 34, 323–329
- Pruppacher H. R. and J. D. Klett 1997, Microphysics of clouds and precipitation, Springer, New York.
- Swanson, B. D., N. J. Bacon, E. J. Davis and M. B. Baker 1999: Electrodynamic trapping and manipulation of ice crystals. Q. J. R. Meteorol. Soc., 125, 1039–1058
- Westbrook, C. D., R. C. Ball, P. R. Field and A. J. Heymsfield 2004: Universality in snowflake aggregation. Geophys. Res. Lett., 31, L15104–15107
- Westbrook, C. D., R. J. Hogan, A. J. Illingworth and E. J. O'Connor 2006: Theory and observations of ice particle evolution in cirrus using Doppler radar: evidence for aggregation. Submitted to Geophys. Res. Lett.
- Wilson, D. R. and S. P. Ballard 1999: A microphysically based precipitation scheme for the UK Meterological Office Unified Model, Q. J. R. Meteorol. Soc., 125, 1607–1636
- Wintle, H. J. 2004: The capacitance of the cube and square plate by random walk methods, *J. Electrostatics*, **62**, 51–62
- Witten, T. A. and L. M. Sander 1981: Diffusion limited aggregation, a kinetic critical phenomenon, *Phys. Rev. Lett.*, 47, 1400–1403
- Woods, C. P., M. T. Stoelinga, J. D. Locatelli and P. V. Hobbs 2006: The IMPROVE-1 Storm of 1-2 February 2001. Part III: Sensitivity of a mesoscale model simulation to the representation of snow particle types and testing of a bulk microphysical scheme with snow habit prediction. J. Atmos. Sci., in press.